JGR Planets

RESEARCH ARTICLE
10.1029/2020JE006565

Geologically Old but Freshly Exposed Rock Fragments Encountered by Yutu-2 Rover

Sheng Gou[1,2,3], Zongyu Yue[1,4], Kaichang Di[1,4], Roberto Bugiolacchi[2,3,5], Wenhui Wan[1], Meiping Yang[1,6], and Lejia Ye[1,6]

[1]State Key Laboratory of Remote Sensing Science, Aerospace Information Research Institute, Chinese Academy of Sciences, Beijing, China, [2]State Key Laboratory of Lunar and Planetary Sciences, Macau University of Science and Technology, Macau, China, [3]CNSA Macau Center for Space Exploration and Science, Macau, China, [4]Center for Excellence in Comparative Planetology, Chinese Academy of Sciences, Hefei, China, [5]Earth Sciences, University College London, London, UK, [6]University of Chinese Academy of Sciences, Beijing, China

Key Points:

- Yutu-2 rover observed two rock fragments with different physical attributes from the surrounding surface
- Spectral evidence suggests they might originate from the 73-km Finsen crater, about 140 km away from the finding site
- The fragments might have been brought to the surface about 16 Myr by the ejecta from the 3.8-km Zhinyu crater

Supporting Information:

- Supporting Information S1

Correspondence to:
K. Di,
dikc@radi.ac.cn

Citation:
Gou, S., Yue, Z., Di, K., Bugiolacchi, R., Wan, W., Yang, M., & Ye, L. (2021). Geologically old but freshly exposed rock fragments encountered by Yutu-2 rover. *Journal of Geophysical Research: Planets*, *126*, e2020JE006565. https://doi.org/10.1029/2020JE006565

Received 10 JUN 2020
Accepted 10 FEB 2021

Author Contributions:
Conceptualization: Zongyu Yue, Kaichang Di
Data curation: Meiping Yang, Lejia Ye
Funding acquisition: Sheng Gou, Zongyu Yue, Kaichang Di
Investigation: Meiping Yang
Methodology: Zongyu Yue, Wenhui Wan
Visualization: Meiping Yang
Software: Wenhui Wan
Supervision: Kaichang Di
Writing – original draft: Sheng Gou
Writing – review & editing: Zongyu Yue, Kaichang Di, Roberto Bugiolacchi

Abstract During the exploration traverse of the Von Kármán crater on the lunar farside, the Yutu-2 rover, part of China's Chang'e-4 mission, come across rock fragments with higher albedo than the surrounding surface. This study investigates their origin, emplacement, and composition based on in situ spectral analysis and geological considerations. The spectral signatures of two fragments show a clear dominance of low-calcium pyroxenes against the high-calcium phases characteristic of the basalts infilling the Von Kármán crater. Based on spectral considerations, this suggests an allochthonous origin for the ejecta fragments, with the most likely source attributable to the Imbrian 73-km Finsen crater. We propose that these rock fragments might have had a convoluted history, born as ejected target materials from the Imbrian Finsen impact, possibly buried and resurfaced several times within Von Kármán by the churning mechanisms that continuously reshape the lunar surface, and finally exhumed by a secondary impact from the Copernican 3.8-km Zhinyu crater.

Plain Language Summary Due to widespread micro to macro impacts and diurnal temperature cycling, most exposed rocks on the lunar surface turn into small fragments and dust within a few millions of years, leaving the surface covered by a type of soil, called regolith, with a relatively uniform color and texture. The Yutu-2 rover from China is exploring the floor of the Von Kármán crater on the relatively unknown lunar farside. On 2 days of its journey, a few light-colored rock fragments stood out from the predominantly dark materials making up most of its surface. By analyzing their color and composition through dedicated instruments, it becomes apparent that these rocks are out of place and very similar in composition, at least within one mineral component called pyroxene, to the Imbrian Finsen crater materials. Some fragments string out in long chains around a 15-m elliptical fresh crater, pointing to their origin. Further analysis suggests that these rock fragments might have been buried in the regolith, and then exposed again by a secondary crater formed by ejecta from the "recent" Copernican Zhinyu crater.

1. Introduction

In January 2019, China's Chang'e-4 lander touched down on the floor of Von Kármán crater at (177.588°E, 45.457°S) within the South Pole-Aitken (SPA) basin on the lunar farside. It then deployed a rover called Yutu-2 to conduct measurements along its traverse path (Figure 1). The Von Kármán is a complex crater with an estimated model age of 3.97 Ga (Yingst et al., 2017), a diameter of 186 and a maximum depth of about 2.4 km. The crater was infilled with basalts by several extrusive events during the Imbrian period (Gou et al., 2021a; Huang et al., 2018), each time resetting the low-to-mid-size crater populations. Based on orbital and in situ measured data, the surface materials of the Chang'e-4 landing site are generally thought to represent Imbrian Finsen crater ejecta (e.g., Di et al., 2019; Gou et al., 2019, 2020b; Huang et al., 2018; Lai et al., 2020; Li et al., 2019b; Lin et al., 2020), which has been gardened into mature lunar regolith over billions of years (Gou et al., 2020b).

As of December 21, 2020, the Yutu-2 rover had already operated for 25 lunar days and traversed about 601 m within the Von Kármán crater. During the 3rd (February 28 to March 13, 2019) and 13th (December

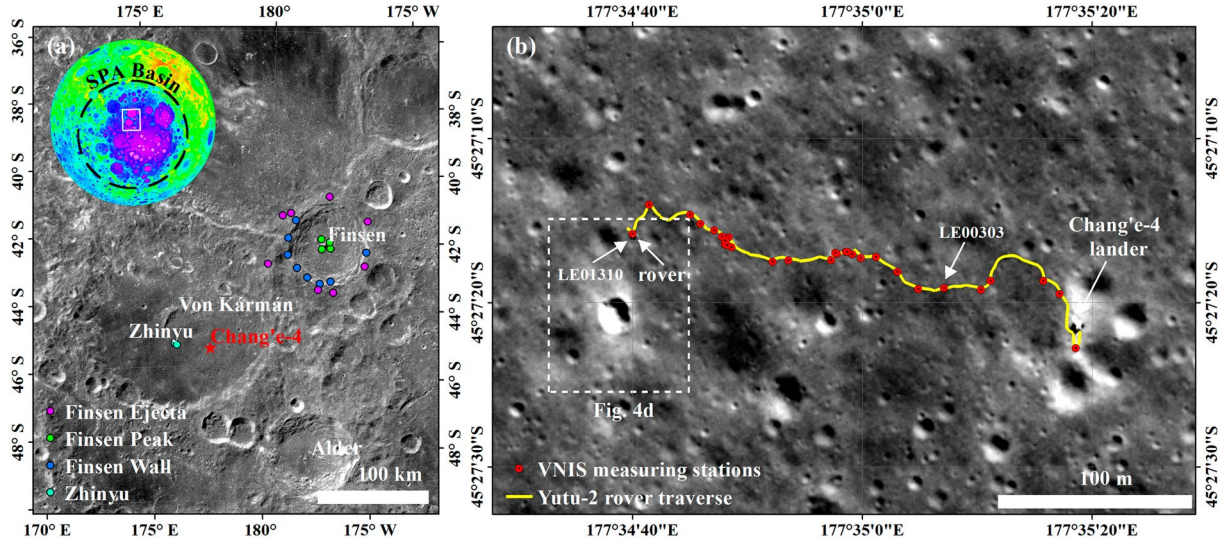

Figure 1. (a) Geologic context of Chang'e-4 landing site, marked by a red star. The base map is a digital orthophoto map mosaic (~7 m/pixel) generated from Chang'e-2 images (Ren et al., 2014). The Lunar Orbiter Laser Altimeter (LOLA) topography elevation (Smith et al., 2010) inset shows the extent of the figure (white box) within the SPA basin. Colors represent different heights in the inset, with red being the highest and purple the lowest. Dots with different colors correspond to locations of Moon Mineralogy Mapper (M^3) spectra, which are used for spectral comparison (see Section 2.3). This figure is modified after Figure 1 in Gou et al. (2020c); (b) Traverse map of Yutu-2 rover over the past 13 lunar days. The base map is a Lunar Reconnaissance Orbiter Camera (LROC) Narrow Angle Camera (NAC; Robinson et al., 2010) image (~1 m/pixel), which was acquired on December 24, 2019 (ID: M1331814485LE). SPA, South Pole-Aitken.

20, 2019 to January 2, 2020) lunar days, the Yutu-2 rover encountered unusual rock fragments of various sizes, characterized by higher albedo than the background. Due to the combined entropic action of micro to macro impacts and the extreme thermal excursions in the airless lunar environment, most exposed rock fragments on the floor of Von Kármán crater should have been fragmented over millions of years (Basilevsky et al., 2013; Hörz et al., 1975; Molaro & Byrne, 2012), leaving the surface covered by a compacted layer of regolith (agglutinated fragments) and dust, with a largely uniform color and texture.

To unravel the origin and composition of the rock fragments, we analyzed images and spectra acquired by the panoramic camera (Pancam) and visible/near-infrared spectrometer (VNIS) instruments onboard the Yutu-2 rover. This work aims at improving our understanding of the evolution of regolith in the vicinity of the Chang'e-four landing site within the Von Kármán crater.

2. Data

2.1. Pancam Images

The Pancam instrument, mounted on the mast of Yutu-2 rover, is composed of two cameras with identical functions, performances, and interfaces (Jia et al., 2018). Each camera has a stereo baseline of 270 mm and acquires an image in a spectral range of 420–700 nm, with a horizontal and vertical field of views (FOVs) being 19.7° and 14.6°, respectively (Jia et al., 2018). The effective image size is 2,352 × 1,728 pixels in color mode and 1,176 × 864 pixels in panchromatic mode. The Pancam has an angular resolution of 0.15 mrad (about 120 pixels/degree), thus the spatial resolution of the Pancam image depends strongly on the distance from the camera (rover). When the rover stops at a certain waypoint, the Pancam takes 28 pairs of stereo images at a pitch angle to produce a 360° panoramic view for location-awareness, terrain reconstruction, and path planning. To cover a larger vertical FOV, Pancam sometimes acquires images at two or three pitch angles (Liu et al., 2020).

Pancam acquired stereo images during the 3rd and 13th lunar day before making in situ spectral measurements. Pancam mosaic is generated from these images for visual perception of the surrounding environment at each rover waypoint (Figure 2). The spatial distribution and size of the encountered rock fragments are determined and measured from the Pancam stereo images using an in-house developed photogrammetric

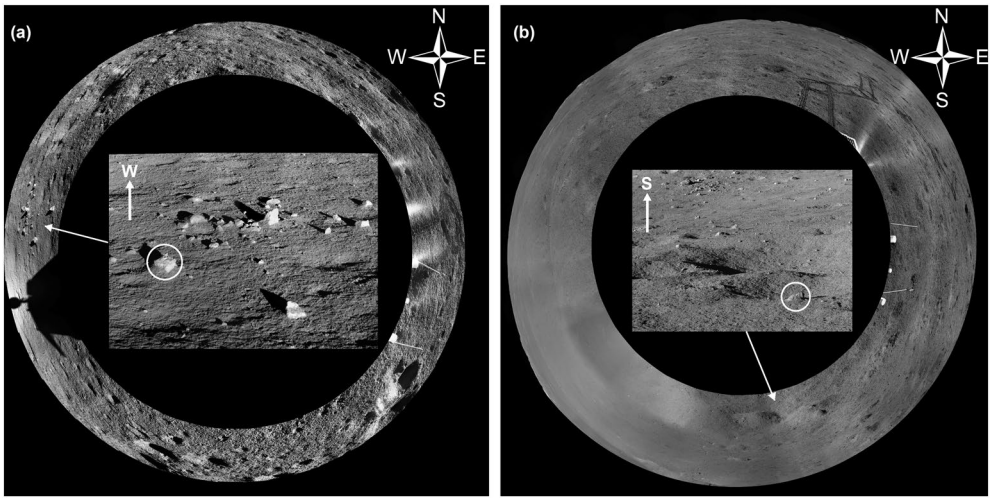

Figure 2. Rock fragments encountered by the Yutu-2 rover. (a and b) are Pancam mosaics generated from Pancam's left-eye images acquired during the 3rd and 13th lunar day, respectively. The targeted fragments at waypoints LE00303 and LE01310 for spectral measurements are indicated by white circles in each Pancam image. The width of each rover rut is 15 cm, and the tread of the rover is about 85 cm. They can be used as scale references in both mosaics.

mapping software (Di et al., 2016). Note that the size discussed in this study is the apparent width, which is calculated as the distance between the leftmost and rightmost ends of the rock fragment's visible facies.

2.2. In Situ Measured Spectra

The VNIS instrument includes a visible/near-infrared (VIS/NIR) imaging spectrometer in the range 450–945 nm with a spectral resolution of 2–7 nm, a shortwave infrared (SWIR) detector that works from 900 to 2,395 nm with a spectral resolution of 3–12 nm, and a white panel for calibration and dust-proofing (Li et al., 2019b). The effective image size of the VIS/NIR imaging spectrometer is 256 × 256 pixels, and the spatial resolution is ~1 mm/pixel typically from 1 m distance. The FOV of the SWIR detector corresponds to a circular region in the VIS/NIR image with the center located at (96, 128) and a radius of 54 pixels (Li et al., 2019b).

To ensure the safety of the Yutu-2 rover, the selection of the observation target is determined by the teleoperation team. Therefore, as of the end of the 13th lunar day, the VNIS only made in situ spectral measurements on two rock fragments at waypoints LE00303 and LE01310, respectively. The key observation target at the rest VNIS observation waypoints was the regolith, in particular, the wheel-trenched regolith compared to the background (a VNIS observation summary is provided as Table S1). The measured raw data were preprocessed and released to the public as level 2B radiance spectra. The radiance spectra were then processed to derive the full-range reflectance spectra (450–2,395 nm) by the solar irradiance calibration method (Gou et al., 2019) for further analysis. The spectra of the two rock fragments (i.e., LE00303 and LE01310) and examples of their surrounding regolith (i.e., LE00304 and LE01305) are shown in Figure 3. The average albedos of the rock fragments at waypoints LE00303 and LE01310 are 0.1747 and 0.1966, respectively, while the average albedos of the regolith at waypoints LE00304 and LE01305 are 0.0926 and 0.1265, respectively. These values are consistent with the observation that rock fragments typically have higher albedos than the regolith of similar composition (Pieters & Englert, 1993).

2.3. Moon Mineralogy Mapper Spectra

The Moon Mineralogy Mapper (M^3) that flew onboard India's Chandrayaan-1 lunar orbiter, was a push-broom imaging spectrometer operating from the visible into the NIR (0.42–3.0 μm). M^3 observed the lunar surface either in a high-resolution target mode (80 m/pixel; 260 spectral channels) or in a low-resolution global mode (140 m/pixel; 85 spectral channels) from a 100 km orbit (Pieters et al., 2009). The M^3 Level 2

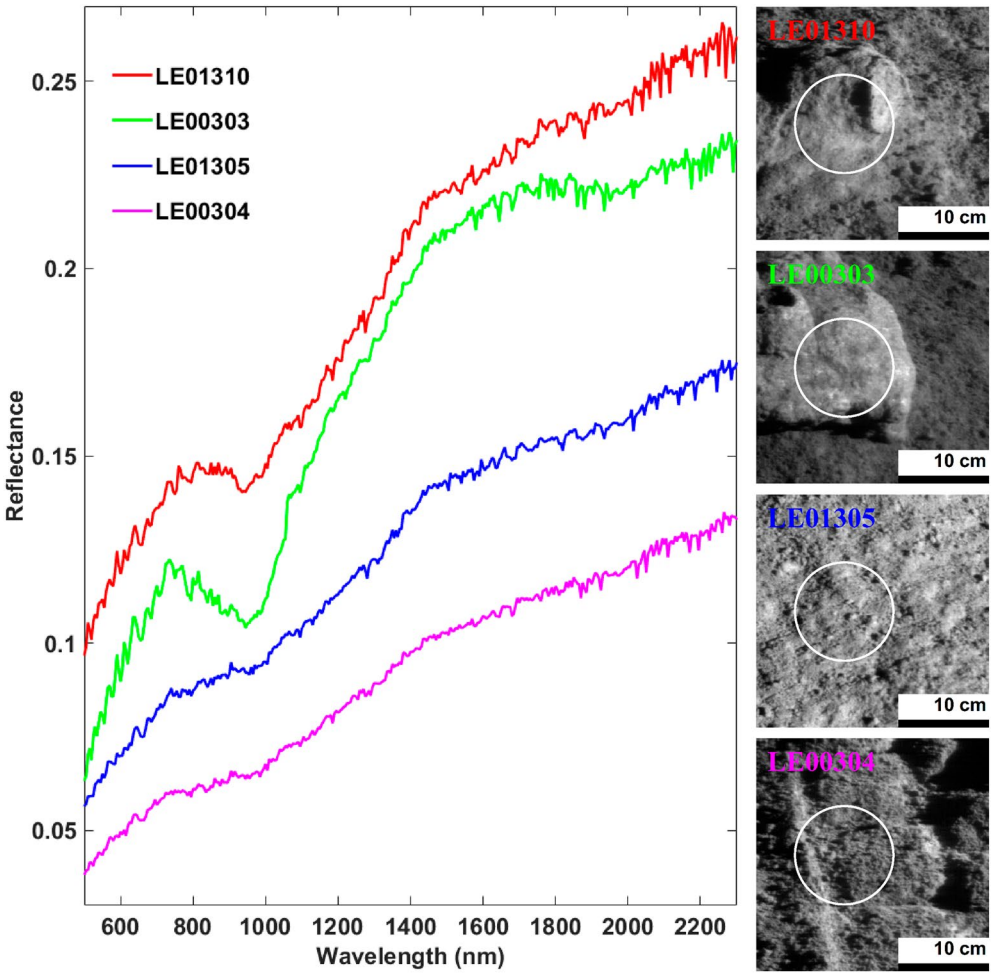

Figure 3. Spectra of rock fragments and examples of their surrounding regolith measured by the VNIS. The white circle in each image indicates the FOV of the SWIR detector. FOV, field of view; SWIR, shortwave infrared; VNIS, visible/near-infrared spectrometer.

spectral reflectance images (REFIMG), which have been photometrically calibrated and thermal emission corrected (Besse et al., 2013; Clark et al., 2011), are used in this study.

The surface materials observed by the Yutu-2 rover are generally thought to be Finsen crater ejecta, not the underlying mare basalts (e.g., Di et al., 2019; Gou et al., 2019, 2020a; Huang et al., 2018; Lai et al., 2020; Li et al., 2019a; Lin et al., 2020). Finsen crater (42.29°S, 177.72°W), ~ 73 km in diameter and lying northeast of Von Kármán crater, is a well-preserved complex crater that has a prominent central peak (Figure 1). Zhinyu crater (176.15°E, 45.34°S), ~3.8 km in diameter and lying northwest of Chang'e-4 landing site (Figure 1), is a fresh simple crater that penetrates the mare basalts inside the host crater. To compare the spectra of the rock fragments with those of attributed to the Finsen crater materials and mare basalts exposed by the Zhinyu crater, M^3 spectra from Zhinyu crater and different locations of Finsen crater (Figure 1), including Finsen crater central peak, wall, and ejecta, were extracted (3-by-3 pixel averages).

3. Methods

3.1. Analysis of Spectral Absorption Features

Both rock fragments spectra show absorptions around 1,000 and 2,000 nm (Figure 3), which are the indicators of the presence of pyroxene minerals. Generally, orthopyroxene (OPX) has absorptions features centered at ~900 and ~1,900 nm while clinopyroxene (CPX) has absorptions at shorter frequencies, ~1,000 and

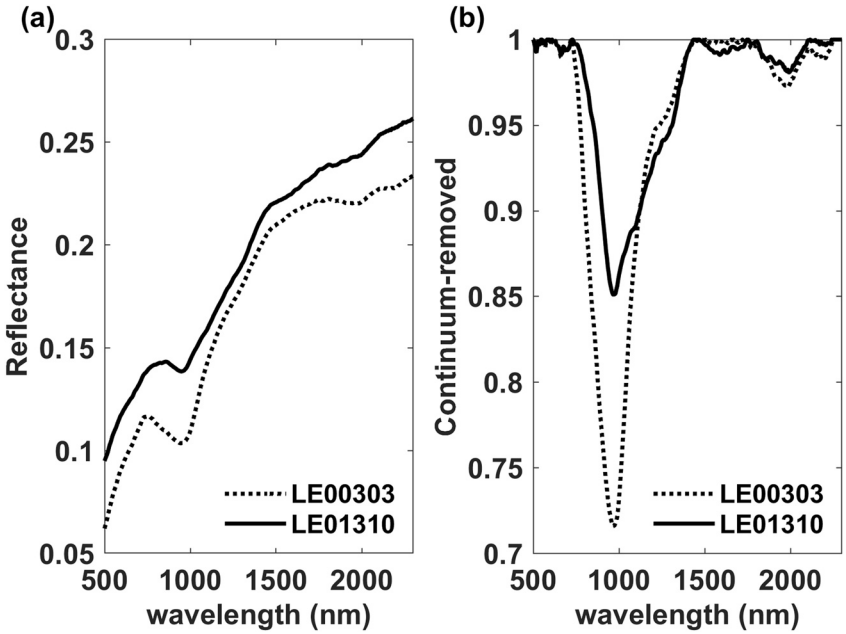

Figure 4. Spectra of rock fragments measured at waypoints LE00303 and LE01310, respectively. (a) Smoothed; (b) Continuum-removed.

~2,200 nm (Adams, 1974). Therefore, the exact absorption positions, also known as band centers, around 1,000 and 2,000 nm, often referred to as the "one- and two-micron features," of both M^3 and VNIS spectra are calculated based following the removal of the "continuum." This technique was developed to amplify weak absorption features, often due to the presence of opaque fractions within the sample, such as nanometer-scale particles of metallic iron (npFe°) within the regolith. Their presence, which accumulates in time with exposure to cosmic weathering, tends to "flatten the curve" (i.e., the absorption features strength) and "redden the continuum slope" (i.e., increase reflectance in the NIR; Hapke et al., 1975; Morris, 1980). Using this approach, the spectra are smoothed by a Savitzky-Golay filter (Savitzky & Golay, 1964) with a 15-point quadratic polynomial (Figure 4). Next, a straight-line continuum is applied in this study by selecting the reflectance maxima on either side of each absorption region, which removes any spectral slope effects due to phase angle differences (Mitchell et al., 2020). The three reflectance maxima of a rock fragment spectrum are generally around 750, 1,500 and 2,350 nm (Figure 4). Third, a second-order polynomial fit is then made to the continuum-removed spectral values around each absorption region, and the minimum of the polynomial is determined to be the band center.

3.2. Determination of Absolute Model Age

Based on our interpretations of the data as discussed in sections 4.3 and 4.4, the spectral features of the two rock fragments are comparable to those of surface materials of Imbrian associated to the Finsen crater. They might represent freshly exposed rock fragments by a secondary impact from Zhinyu crater. To estimate the exposure time of these rock fragments, an absolute model age (AMA) of Zhinyu crater was derived using crater size-frequency distribution (CSFD) analysis, which combines information from crater formation rates and radiometric ages of lunar rock samples (Neukum, 1983). The CSFD data were obtained following these steps: (1) outline a representative area of the Zhinyu crater ejecta blanket; (2) map craters using CraterTools (Kneissl et al., 2011), an application written for the ArcGIS software, within the outlined representative area. Due to the inherent uncertainties in diameter measurements (~10%; Robbins et al., 2014; Wang et al., 2020), only craters with diameters larger than 5 m were utilized; (3) compare the CSFD of the area to lunar chronology models (Neukum, 1983) after randomness analysis (Michael et al., 2012). This step was carried out utilizing Craterstats (Michael & Neukum, 2010; Michael et al., 2012). Further information on

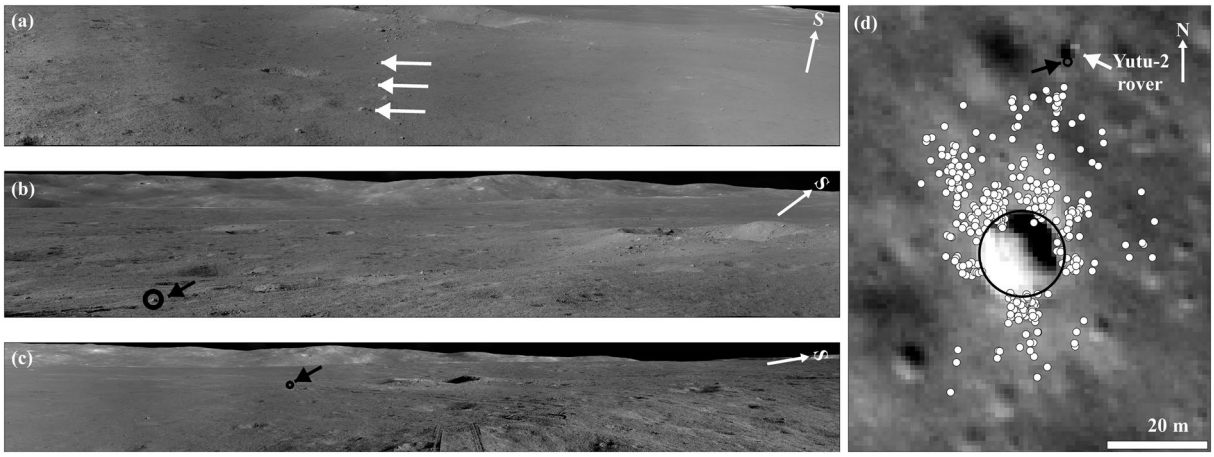

Figure 5. (a–c) Pancam mosaics of the 15-m fresh crater with a blocky rim. These mosaics were produced from Pancam's left-eye images acquired during the 13th, 14th, and 15th lunar day, respectively. The white arrows in (a) mark one of the rock fragments chains. (d) The spatial distribution of rock fragments around the 15-m crater. Each white dot represents a rock fragment. The base map is the same as that of Figure 1b. The Yutu-2 rover approached the rock fragment for a close VNIS observation at waypoint LE01310 and then withdrew during the 13th lunar day. Due to the Pancam's viewing geometry (the rock fragment is very close to the Pancam/rover), the VNIS measured rock fragment cannot be seen on the Pancam mosaic shown in (a). The location of the VNIS observed rock fragment is marked by the black circle with an arrow in (b–d). VNIS, visible/near-infrared spectrometer

the application of CSFD measurements to determine the AMA of Zhinyu crater is found in the supplementary material.

4. Results and Discussions

4.1. Distribution of Rock Fragments

Three Pancam mosaics (Figures 5a–5c), produced from left-eye images acquired during the 13th, 14th, and 15th lunar day, respectively, show that rock fragments encountered at waypoint LE01310 mostly cluster around a ~15 m impact crater. A sharp rim and abundant ejecta are indicators of crater freshness (Basilevsky, 1976; Basilevsky et al., 2013; Fassett & Thomson, 2014; Hörz et al., 1975). The 15-m crater has indeed a well-defined rim with many rock fragments scattered across the whole morphology, both in and outside (Figures 5a–5c) the impact, suggesting a relatively young age.

Due to the shooting angle of the Pancam, most of the area south of the 15-m impact crater is within a blind area. Nevertheless, rock fragments are distributed radially around the 15-m impact crater, with density decreasing with distance from the crater rim (Figure 5d). Craters devoid of rock fragments form solely within the loose and unconsolidated regolith layer, and craters with blocks are an indicator of (partially) penetration of a coarse-grained or coherent bedrock layer (Wilcox et al., 2005). Rock fragments at waypoint LE01310 string out in long chains in multiple directions and extend more than two crater radii from the rim crest (Figure 5d), indicating a common origin. A Pancam mosaic shows the orientation of one of the chains extends northwest-southeastward (Figure 5a). The observed rock fragments radiating in different directions are thus essentially chain clusters of ejecta from the 15-m impact crater. The evidence points to a crater that was excavated on a target consisting of a loose and unconsolidated regolith layer over a coarse-grained or possibly a coherent layer (bedrock) which was (partially) penetrated during crater formation.

Unlike what is observed for the rock fragments at waypoint LE01310 (Figure 1b), the distribution of rock fragments at waypoint LE00303 cannot be related to their surroundings based on the Pancam mosaic (Figure 2a). Therefore, it is impossible to determine their spatial distribution.

4.2. Implications for Local Regolith

Much of the evidence proposes that the Chang'e-4 landing site was covered by ejecta from Finsen crater (e.g., Di et al., 2019; Gou et al., 2019, 2020a; Huang et al., 2018; Lai et al., 2020; Li et al., 2019a; Lin et al., 2020).

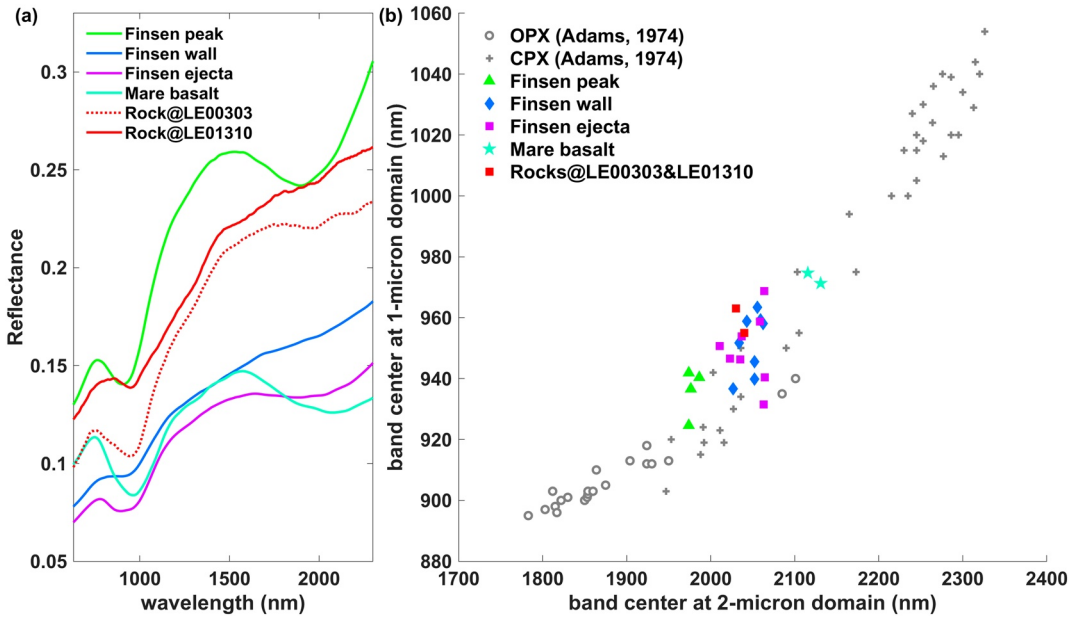

Figure 6. Spectral features of the Finsen crater materials, basalts exposed by the Zhinyu crater, and the two rock fragments measured by the Yutu-2 rover. (a) Smoothed spectra. Only 1 M^3 spectrum of each type is shown here, and the rest are available from the data repository; (b) absorption band centers comparison.

After deposition of Finsen ejecta, the surface of the landing site has been impacted and gardened by meteorites for billions of years. As a result, a fine-grained unconsolidated layer termed "regolith" accumulated gradually above a coarse-grained or even coherent (e.g., bedrock) layer. If one impact penetrates through the fine-grained regolith layer, it will excavate materials in the underlying layer and deposit them around the crater. Therefore, the thickness of regolith could be estimated from the excavation depth of the smallest crater with a blocky rim (Wilcox et al., 2005), like the one encountered at waypoint LE01310.

For a simple crater on the lunar surface, its maximum excavation depth (H_{exc}) is approximately equal to 1/10 the transient crater diameter (D_t), which is about 0.84 times of the crater rim-to-rim diameter (D), that is, $H_{exc} = 0.1D_t = 0.084D$ (Melosh, 1989). After checking all the available Pancam images, no other crater with obvious rock fragments around its rim was observed. The 15-m crater becomes the only example in this area. Because rock fragments are exposed during the impact-cratering process, it is likely that the thickness of local fine-grained loose regolith at waypoint LE01310 should be no more than 1.3 m, which is calculated from maximum excavation depth of the 15-m crater. However, previous works reported that the thickness of a regolith layer at Chang'e-4 landing site is about 12 m, which is derived from the 500 MHz high-frequency lunar penetrating radar (LPR) data (Lai et al., 2019; Li et al., 2020). It is unlikely that the local thickness of the lunar regolith would differ so drastically from the average. One possible scenario to explain the difference of nearly an order of magnitude is that there might be abundant rock fragments admixed in the regolith, which would have been exposed by the impact event. No rock fragments smaller than 1 cm are measured in this study, due to limited resolution of the Pancam images. Measurements reveal that the mean and variance of the sizes of rock fragments are about 7.3 and 5.9 cm, respectively. However, the resolution of the high-frequency LPR data is about 17 cm (Li et al., 2018). Therefore, these buried rock fragments may not be visible in the LPR radargram. Another possible explanation might be rooted in semantics, in terms of the definition of regolith between this study and the works of Lai et al. (2019) and Li et al. (2020), that is, fine-grained regolith versus regolith with coarse rock fragments embedded inside.

4.3. Source of Rock Fragments

Spectral analysis reveals the absorption features of the two rock fragments are similar to that of Finsen crater materials (rich in low-calcium pyroxene) and are clearly compositionally different from that of the underlying mare basalts (rich in high-calcium pyroxene) excavated by the Zhinyu crater (Figure 6). It is

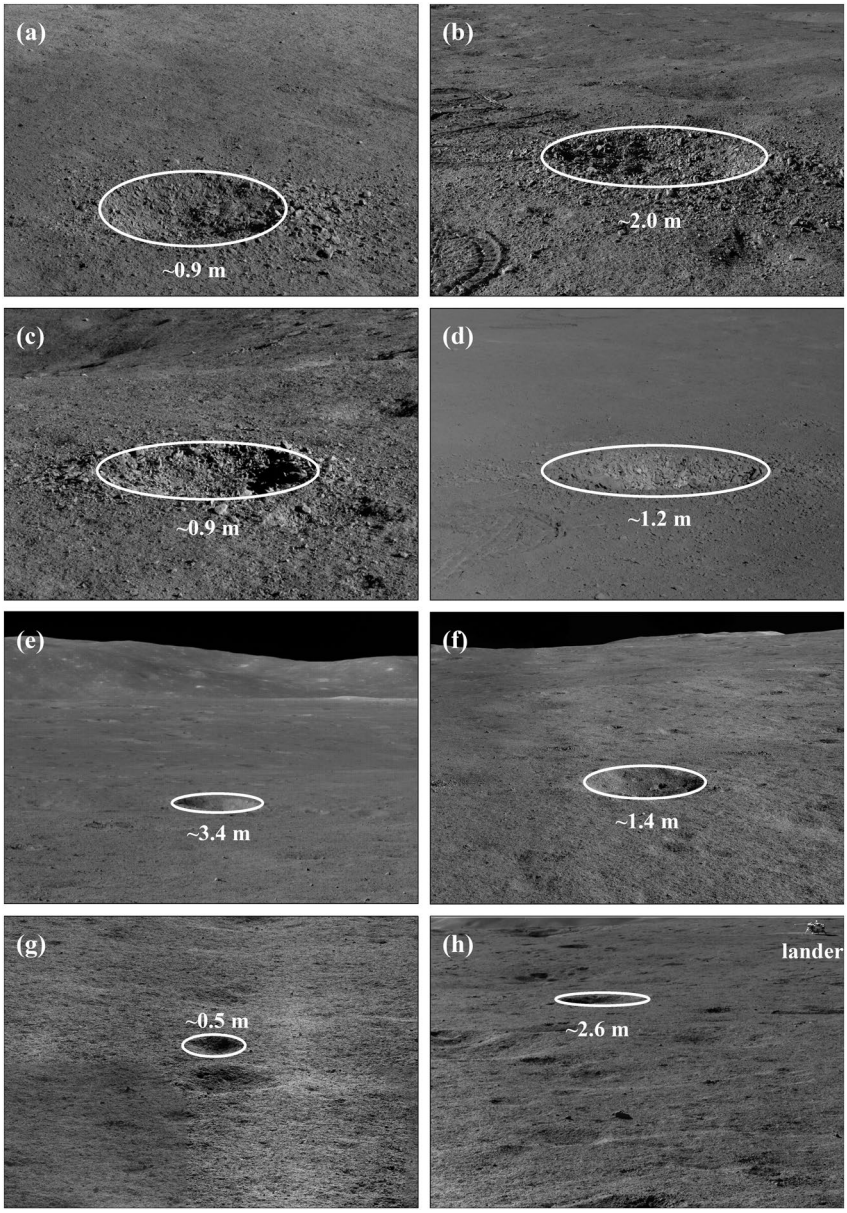

Figure 7. Pancam images of fresh craters (a–d) and heavily degraded craters (e–h) in the Chang'e-4 landing area. Because the spatial resolution of the Pancam image depends strongly on distance from the camera (rover), the size of each crater is marked as an alternative for scale bar. The rover wheel rut seen in (b and d) is 15 cm wide.

reasonable to deduce that these buried rock fragments might also be ejecta from the Finsen crater, which is Imbrian (Ivanov et al., 2018; Gou et al., 2021b). The sizes of the two rock fragments are about 25 and 20 cm, respectively. Survival times of meter-sized rocks on the lunar surface is usually no more than 300 Ma (Basilevsky et al., 2013). Very few examples of micrometeorite impacts are observed in the close-up images (Figure 3), which leads to the inference that the rocks fragments have been exposed to space weathering for a relatively short geological time. We conclude that the Yutu-2 rover might have stumbled across rock fragments that were buried within the regolith with time, maybe several times, before eventually being exhumed and redeposited on the surface. This is also supported by the observation that both rock fragments show limited space weathering effects with strong mafic absorption features (Figure 3; Pieters & Noble, 2016): A heavily space weathered rock fragment would have developed a thick patina coating, whose

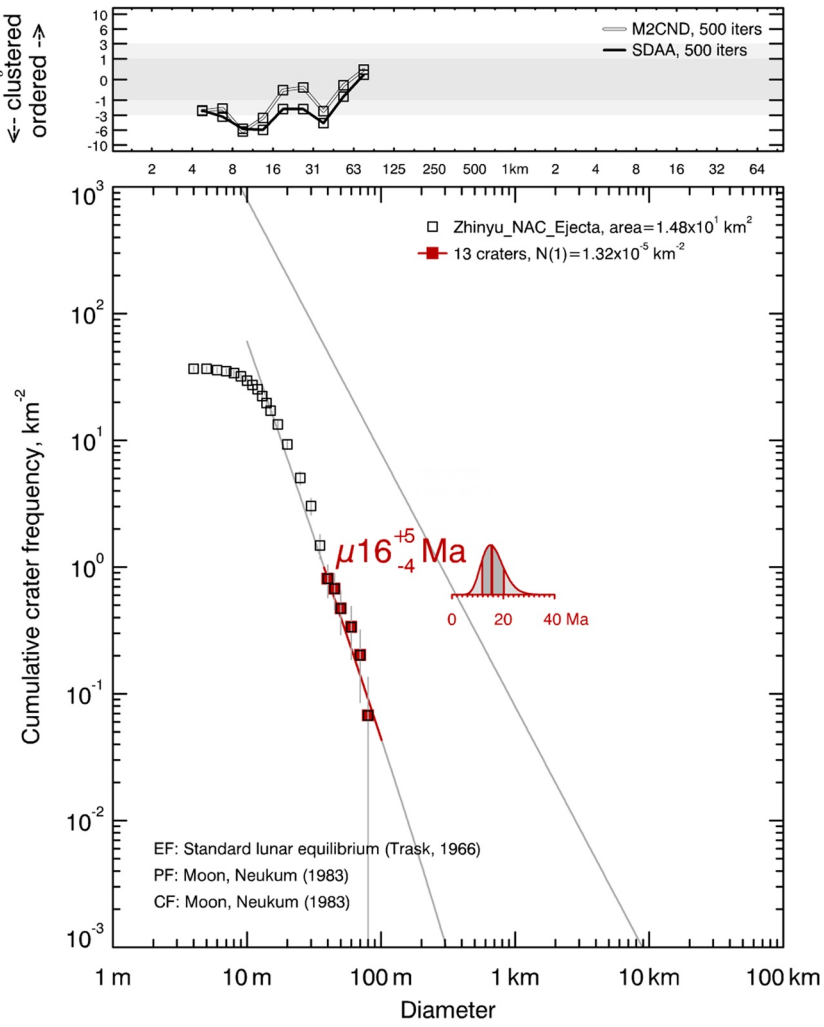

Figure 8. Absolute model age of Zhinyu crater. According to randomness analysis, craters with a diameter ≥40 m are used for fitting and are marked as red filled squares.

spectral reflectance properties would differ from that of the underlying rock (Frushour et al., 2014; Morrison et al., 1973; Wentworth et al., 1999).

4.4. The Exposure Time of Rock Fragments

The 15-m fresh crater is not the only crater visited by the rover during its traverse inside the Von Kármán crater. Along with heavily degraded craters, there are many fresh craters with blocky rims and interiors in this area (Figure 7). Some of the small blocks around these fresh craters were pulverized by the rover's wheels and their derived composition show similarities with the surrounding Finsen ejecta-sourced regolith, indicating these blocks to be regolith conglomerates (not cohesive rock fragments) possibly belonging to the Finsen ejecta (Gou et al., 2020c). Considering the fast regolith growth rate at the Chang'e-4 landing site (Gou et al., 2021b; Lai et al., 2019) and quick breakdown of boulders on the lunar surface (Basilevsky et al., 2013), the high spatial density of these fresh craters in such a small region is not typical of primary craters (Ding et al., 2020).

Zhinyu crater (176.15°E, 45.34°S), ~3.8 km in diameter and ~800 m in depth, is a fresh simple crater that has a faint impact ray system extending to the Chang'e-4 landing site (Ding et al., 2020). Ejecta from craters such as Zhinyu would cause secondary craters, which are usually elongated radially with respect to

the primary crater and form shallow depressions, crater chains, and crater clusters (e.g., McEwen & Bierhaus, 2006). The axis lengths of northwest-southeast and southwest-northeast directions of the 15-m crater under investigation are ~18 and ~15 m, respectively, indicating the impact direction might be northwest-southeastward. These considerations point to the most likely origin as an elliptical secondary crater by ejecta from the Zhinyu crater. CSFD measurement on ejecta blanket of the Zhinyu crater yields an AMA of μ16 (+5, −4) Ma (Figure 8). Therefore, the rock fragments encountered by the Yutu-2 rover during the 13th lunar day might be buried Imbrian Finsen crater materials that were freshly exposed by a secondary crater formed by ejecta from the 10–20-Ma-old Zhinyu crater.

5. Conclusion

The Yutu-2 rover, part of the Chang'e-4 lunar mission to the lunar farside, come across rock fragments during its traverse of the Von Kármán crater floor. Two rock fragments were studied using spectral analysis at waypoints LE00303 and LE01310 (Figure 1b). Their spectral absorption characteristics were found to differ from the surrounding mare basalts, but rather to resemble those from the Finsen crater materials derived through remote sensing (rich in low-calcium pyroxene), indicating these rock fragments might be related to the impact.

The rock fragments encountered at waypoint LE01310 are distributed around ~15 m impact crater, which appears relatively fresh. Some of the rock fragments line up in long chains radiating on multiple directions extending more than two crater radii from the rim crest, indicating a common origin. The Zhinyu crater is a fresh simple crater that has an optically faint impact ray system that can be traced up to the Chang'e-4 landing site. Ejecta from Zhinyu crater also excavated secondary craters with an asymmetric axis with the longer pointing back at the source. The axis lengths of northwest-southeast and southwest-northeast directions of the 15-m crater are ~18 and ~15 m, respectively, suggesting that the crater most likely represents an elliptical secondary crater formed by the low-angle ejecta from the Zhinyu crater.

The observed rock fragments represent a subset of the ejecta from the 15-m impact crater, suggesting the target to be a fine-grained unconsolidated regolith layer overlaying a coarser-grained or even coherent layer, which was (partially) penetrated during crater formation. CSFD measurement on the Zhinyu crater's ejecta blanket yields an AMA of μ16 Ma. We propose that these rock fragments might be traced to buried Imbrian Finsen crater materials, which were freshly exhumed by a secondary crater formed by the ejecta from the Zhinyu crater.

Conflict of Interest

The authors declare that they have no known competing financial interests or personal relationships that could have appeared to influence the work reported in this article.

Acknowledgments
The authors gratefully thank the whole Chang'e-4 team for making the mission a great success. This work was supported by the Strategic Priority Research Program of Chinese Academy of Sciences (grant No. XDB41000000), National Natural Science Foundation of China (Grant Nos. 41702354 and 41941003), Macao Young Scholars Program (grant No. AM201902), and Science and Technology Development Fund of Macau (grant No. 131/2017/A3). The authors thank Prof. Alexander T. Basilevsky, Dr. Noah Petro and an anonymous reviewer for their constructive comments and suggestions that improved the quality of the paper substantially. We also thank Dr. Bradley Thomson and Dr. Wenzhe Fa for the efficient and helpful editorial handling.

Data Availability Statement

The Chang'e-4 scientific data are provided by the China National Space Administration (CNSA), and are available through the data release and information service system of China's Lunar Exploration Program (CLEP) (http://moon.bao.ac.cn/searchOrder_dataSearchData.search). The M^3 and LROC NAC images are available from the Lunar Orbital Data Explorer in the PDS Geoscience Node (https://ode.rsl.wustl.edu/moon/indexProductSearch.aspx). The image IDs for producing Figures 1–7 and the derived data presented in Figures 6 and 8 are available at the data repository (http://doi.org/10.5281/zenodo.4018823).

References

Adams, J. B. (1974). Visible and near-infrared diffuse reflectance spectra of pyroxenes as applied to remote sensing of solid objects in the solar system. *Journal of Geophysical Research*, *79*(32), 4829–4836. https://doi.org/10.1029/JB079i032p04829

Basilevsky, A. T. (1976). On the evolution rate of small lunar craters. In *7th lunar science conference*. Houston, TX.

Basilevsky, A. T., Head, J. W., & Horz, F. (2013). Survival times of meter-sized boulders on the surface of the Moon. *Planetary and Space Science*, *89*, 118–126. https://doi.org/10.1016/j.pss.2013.07.011

Besse, S., Yokota, Y., Boardman, J., Green, R., Haruyama, J., Isaacson, P., et al. (2013). One Moon, many measurements 2: Photometric corrections. *Icarus*, *226*(1), 127–139. https://doi.org/10.1016/j.icarus.2013.05.009

Clark, R. N., Pieters, C. M., Green, R. O., Boardman, J. W., & Petro, N. E. (2011). Thermal removal from near-infrared imaging spectroscopy data of the Moon. *Journal of Geophysical Research*, *116*(E6), E00G16. https://doi.org/10.1029/2010JE003751

Di, K., Xu, B., Peng, M., Yue, Z., Liu, Z., Wan, W., et al. (2016). Rock size-frequency distribution analysis at the Chang'E-3 landing site. *Planetary and Space Science*, *120*, 103–112. https://doi.org/10.1016/j.pss.2015.11.012

Di, K., Zhu, M.-H., Yue, Z., Lin, Y., Wan, W., Liu, Z., et al. (2019). Topographic evolution of Von Kármán crater revealed by the lunar rover Yutu-2. *Geophysical Research Letters*, *46*(22), 12764–12770. https://doi.org/10.1029/2019GL085252

Ding, C., Xiao, Z., Wu, B., Li, Y., Prieur, N. C., Cai, Y., et al. (2020). Fragments Delivered by Secondary Craters at the Chang'E-4 Landing Site. *Geophysical Research Letters*, *47*(7), e2020GL087361. https://doi.org/10.1029/2020GL087361

Fassett, C. I., & Thomson, B. J. (2014). Crater degradation on the lunar maria: Topographic diffusion and the rate of erosion on the Moon. *Journal of Geophysical Research: Planets*, *119*(10), 2255–2271. https://doi.org/10.1002/2014JE004698

Frushour, A., Noble, S., Christoffersen, R., & Keller, L. P. (2014). Alteration of lunar rock surfaces through interaction with the space environment. In *45th lunar and planetary science conference*. Houston, the Woodlands.

Gou, S., Di, K., Yue, Z., Liu, Z., He, Z., Xu, R., et al. (2019). Lunar deep materials observed by Chang'e-4 rover. *Earth and Planetary Science Letters*, *528*, 115829. https://doi.org/10.1016/j.epsl.2019.115829

Gou, S., Di, K., Yue, Z., Liu, Z., He, Z., Xu, R., et al. (2020a). Forsteritic olivine and magnesium-rich orthopyroxene materials measured by Chang'e-4 rover. *Icarus*, *345*, 113776. https://doi.org/10.1016/j.icarus.2020.113776

Gou, S., Yue, Z., Di, K., Bugiolacchi, R., Zhu, M.-H., Pinet, P. C., & Cai, Z. (2021a). Mare basalt flooding events surrounding Chang'e-4 landing site as revealed by Zhinyu crater ejecta. *Icarus*, *360*, 114370. https://doi.org/10.1016/j.icarus.2021.114370

Gou, S., Yue, Z., Di, K., Cai, Z., Liu, Z., & Niu, S. (2021b). Absolute model age of lunar Finsen crater and geologic implications. *Icarus*, *354*, 114046. https://doi.org/10.1016/j.icarus.2020.114046

Gou, S., Yue, Z., Di, K., Wan, W., Liu, Z., Liu, B., et al. (2020b). In situ spectral measurements of space weathering by Chang'e-4 rover. *Earth and Planetary Science Letters*, *535*, 116117. https://doi.org/10.1016/j.epsl.2020.116117

Gou, S., Yue, Z., Di, K., Wang, J., Wan, W., Liu, Z., et al. (2020c). Impact melt breccia and surrounding regolith measured by Chang'e-4 rover. *Earth and Planetary Science Letters*, *544*, 116378. https://doi.org/10.1016/j.epsl.2020.116378

Hapke, B., Cassidy, W., & Wells, E. (1975). Effects of vapor-phase deposition processes on the optical, chemical, and magnetic properties OE the lunar regolith. *The Moon*, *13*(1), 339–353. https://doi.org/10.1007/BF00567517

Hörz, F., Schneider, E., Gault, D. E., Hartung, J. B., & Brownlee, D. E. (1975). Catastrophic rupture of lunar rocks: A Monte Carlo simulation. *The Moon*, *13*(1), 235–258.

Huang, J., Xiao, Z., Flahaut, J., Martinot, M., Head, J., Xiao, X., et al. (2018). Geological Characteristics of Von Kármán Crater, Northwestern South Pole-Aitken Basin: Chang'E-4 Landing Site Region. *Journal of Geophysical Research: Planets*, *123*(7), 1684–1700. https://doi.org/10.1029/2018JE005577

Ivanov, M. A., Hiesinger, H., van der Bogert, C. H., Orgel, C., Pasckert, J. H., & Head, J. W. (2018). Geologic History of the Northern Portion of the South Pole-Aitken Basin on the Moon. *Journal of Geophysical Research: Planets*, *123*(10), 2585–2612. https://doi.org/10.1029/2018JE005590

Jia, Y., Zou, Y., Ping, J., Xue, C., Yan, J., & Ning, Y. (2018). The scientific objectives and payloads of Chang'E–4 mission. *Planetary and Space Science*, *162*, 207–215. https://doi.org/10.1016/j.pss.2018.02.011

Kneissl, T., Van Gasselt, S., & Neukum, G. (2011). Map-projection-independent crater size-frequency determination in GIS environments—New software tool for ArcGIS. *Planetary and Space Science*, *59*(11), 1243–1254. https://doi.org/10.1016/j.pss.2010.03.015

Lai, J., Xu, Y., Bugiolacchi, R., Meng, X., Xiao, L., Xie, M., et al. (2020). First look by the Yutu-2 rover at the deep subsurface structure at the lunar farside. *Nature Communications*, *11*(1), 3426. https://doi.org/10.1038/s41467-020-17262-w

Lai, J., Xu, Y., Zhang, X., Xiao, L., Yan, Q., Meng, X., et al. (2019). Comparison of Dielectric Properties and Structure of Lunar Regolith at Chang'e-3 and Chang'e-4 Landing Sites Revealed by Ground Penetrating Radar. *Geophysical Research Letters*, *46*, 12783–12793. https://doi.org/10.1029/2019GL084458

Li, C., Liu, D., Liu, B., Ren, X., Liu, J., He, Z., et al. (2019a). Chang'E-4 initial spectroscopic identification of lunar far-side mantle-derived materials. *Nature*, *569*(7756), 378–382. https://doi.org/10.1038/s41586-019-1189-0

Li, C., Shuguo, X., Lauro, S., Su, Y., Dai, S., Feng, J., et al. (2018). Pitfalls in GPR Data Interpretation: False Reflectors Detected in Lunar Radar Cross Sections by Chang'e-3. *IEEE Transactions on Geoscience and Remote Sensing*, *56*(3), 1325–1335. https://doi.org/10.1109/TGRS.2017.2761881

Li, C., Su, Y., Pettinelli, E., Xing, S., Ding, C., Liu, J., et al. (2020). The Moon's farside shallow subsurface structure unveiled by Chang'E-4 Lunar Penetrating Radar. *Science Advances*, *6*(9), eaay6898. https://doi.org/10.1126/sciadv.aay6898

Li, C., Wang, Z., Xu, R., Lv, G., Yuan, L., He, Z., & Wang, J. (2019b). The Scientific Information Model of Chang'e-4 Visible and Near-IR Imaging Spectrometer (VNIS) and In-Flight Verification. *Sensors*, *19*(12), 2806. https://doi.org/10.3390%2Fs19122806

Lin, H., He, Z., Yang, W., Lin, Y., Xu, R., Zhang, C., et al. (2020). Olivine-norite rock detected by the lunar rover Yutu-2 likely crystallized from the SPA impact melt pool. *National Science Review*, *7*, 913–920. https://doi.org/10.1093/nsr/nwz183

Liu, Z., Di, K., Li, J., Xie, J., Cui, X., Xi, L., et al. (2020). Landing site topographic mapping and rover localization for Chang'e-4 mission. *Science China Information Sciences*, *63*(4), 140901. https://doi.org/10.1007/s11432-019-2796-1

McEwen, A. S., & Bierhaus, E. B. (2006). The importance of secondary cratering to age constraints on planetary surfaces. *Annual Review of Earth and Planetary Sciences*, *34*(1), 535–567. https://doi.org/10.1146/annurev.earth.34.031405.125018

Melosh, H. J. (1989). *Impact cratering: A geologic process*. New York, NY: Oxford University Press.

Michael, G. G., & Neukum, G. (2010). Planetary surface dating from crater size–frequency distribution measurements: Partial resurfacing events and statistical age uncertainty. *Earth and Planetary Science Letters*, *294*(3), 223–229. https://doi.org/10.1016/j.epsl.2009.12.041

Michael, G. G., Platz, T., Kneissl, T., & Schmedemann, N. (2012). Planetary surface dating from crater size–frequency distribution measurements: Spatial randomness and clustering. *Icarus*, *218*(1), 169–177. https://doi.org/10.1016/j.icarus.2011.11.033

Mitchell, A. M., Reddy, V., Sharkey, B. N. L., Sanchez, J. A., Burbine, T. H., Le Corre, L., & Thomas, C. A. (2020). Constraining ordinary chondrite composition via near-infrared spectroscopy. *Icarus*, *336*, 113426. https://doi.org/10.1016/j.icarus.2019.113426

Molaro, J., & Byrne, S. (2012). Rates of temperature change of airless landscapes and implications for thermal stress weathering. *Journal of Geophysical Research*, *117*(E10), E10011. https://doi.org/10.1029/2012JE004138

Morris, R. V. (1980). Origins and size distribution of metallic iron particles in the lunar regolith. In *11th lunar and planetary science conference*. Houston, TX.

Morrison, D., McKay, D., Fruland, R., & Moore, H. (1973). Microcraters on Apollo 15 and 16 rocks. In *4th lunar science conference*. Houston, TX.

Neukum, G. (1983). *Meteoriten bombardement und Datierung planetarer Oberflächen (German original)*. University of Munich.

Pieters, C. M., Boardman, J., Buratti, B., Chatterjee, A., Clark, R., Glavich, T., et al. (2009). The Moon mineralogy mapper (M3) on Chandrayaan-1. *Current Science*, *96*(4), 500–505.

Pieters, C. M., & Englert, P. A. J. (1993). *Remote geochemical analysis: Elemental, and mineralogical compostion*. New York, NY: Cambridge University Press.

Pieters, C. M., & Noble, S. K. (2016). Space weathering on airless bodies. *Journal of Geophysical Research: Planets*, *121*(10), 1865–1884. https://doi.org/10.1002/2016JE005128

Ren, X., Liu, J. J., Wang, F. F., Wang, W. R., Mu, L. L., & Li, H. H. (2014). *A new lunar global topographic map products from Chang'E-2 stereo camera image data*. Cascais, Portugal. European Planetary Science Congress.

Robbins, S. J., Antonenko, I., Kirchoff, M. R., Chapman, C. R., Fassett, C. I., Herrick, R. R., et al. (2014). The variability of crater identification among expert and community crater analysts. *Icarus*, *234*, 109–131. https://doi.org/10.1016/j.icarus.2014.02.022

Robinson, M. S., Brylow, S. M., Tschimmel, M., Humm, D., Lawrence, S. J., Thomas, P. C., et al. (2010). Lunar Reconnaissance Orbiter Camera (LROC) instrument overview. *Space Science Reviews*, *150*, 81–124. https://doi.org/10.1007/s11214-010-9634-2

Savitzky, A., & Golay, M. J. E. (1964). Smoothing and differentiation of data by simplified least squares procedures. *Analytical Chemistry*, *36*, 1627–1639. https://doi.org/10.1021/ac60214a047

Smith, D. E., Zuber, M. T., Neumann, G. A., Lemoine, F. G., Mazarico, E., Torrence, M. H., et al. (2010). Initial observations from the Lunar Orbiter Laser Altimeter (LOLA). *Geophysical Research Letters*, *37*(18), L18204. https://doi.org/10.1029/2010GL043751

Wang, Y., Xie, M., Xiao, Z., & Cui, J. (2020). The minimum confidence limit for diameters in crater counts. *Icarus*, *341*, 113645. https://doi.org/10.1016/j.icarus.2020.113645

Wentworth, S. J., Keller, L. P., McKAY, D. S., & Morris, R. V. (1999). Space weathering on the Moon: Patina on Apollo 17 samples 75075 and 76015. *Meteoritics & Planetary Sciences*, *34*(4), 593–603. https://doi.org/10.1111/j.1945-5100.1999.tb01366.x

Wilcox, B., Robinson, M., Thomas, P., & Hawke, B. (2005). Constraints on the depth and variability of the lunar regolith. *Meteoritics & Planetary Sciences*, *40*, 695–710. https://doi.org/10.1111/j.1945-5100.2005.tb00974.x

Yingst, R. A., Chuang, F. C., Berman, D. C., & Mest, S. C. (2017). Geologic Mapping of the Planck Quadrangle of the Moon (LQ-29). In *48th lunar and planetary science conference*, the Woodlands, TX.

References From the Supporting Information

Clark, J. D., van der Bogert, C. H., & Hiesinger, H. (2018). Investigating the Mandel'shtam lobate scarp complex. *European Planetary Science Congress*, *12*.

McGetchin, T. R., Settle, M., & Head, J. W. (1973). Radial thickness variation in impact crater ejecta: implications for lunar basin deposits. *Earth and Planetary Science Letters*, *20*(2), 226–236. https://doi.org/10.1016/0012-821X(73)90162-3

Moore, H. J., Hodges, C. A., & Scott, D. H. (1974). *Multiringed basins - illustrated by Orientale and associated features*. Houston, TX. 5th Lunar Science Conference. (pp. 71–100).